Scaled Particle Theory Revisited: New Conditions and Improved Predictions of the Properties of the Hard Sphere Fluid†

Michael Heying and David S. Corti*

School of Chemical Engineering, Purdue University, West Lafayette, Indiana 47907-2100

Received: May 31, 2004; In Final Form: August 23, 2004

We revisit the successful scaled particle theory (SPT) of hard particle fluids, originally developed by Reiss, Frisch, and Lebowitz (*J. Chem. Phys.* **1959,** *31*, 369). In the initial formulation of SPT, five exact conditions were derived that constrained the form of the central function *G*. Only three of these conditions, however, were employed to generate an equation of state. Later, the number of relations used to determine *G* was increased to five (Mandell, M. J.; Reiss, H., *J. Stat. Phys.* **1975**, *13*, 113). The resulting equation of state was an improvement over the original formulation, although its accuracy was still limited at high densities. In an effort to increase the accuracy of SPT predictions, we propose two new formally exact conditions on the form of *G*. These sixth and seventh conditions relate exactly known derivatives of *G* to the slope and curvature of the hard sphere radial distribution function at contact, $g'(\sigma^+)$ and $g''(\sigma^+)$, respectively. To apply the new conditions, we derive, again within the framework of SPT, physically and geometrically based approximations to $g'(\sigma^+)$ and $g''(\sigma^+)$. These additional restrictions on the function *G* yield markedly improved predictions of the pressure, excess chemical potential, and work of cavity formation for the hard sphere fluid, now making SPT competitive with other existing equations of state.

1. Introduction

Scaled particle theory (SPT) of the hard sphere fluid was originally developed over 40 years ago by Reiss, Frisch and Lebowitz.[1] Since then, SPT has been usefully employed in the study of a variety of fluid systems,[2−4] mainly those modeled with hard-core interactions although various results are also applicable to fluids whose particles interact via soft-core intermolecular potentials.[5] SPT is not just limited to the calculation of the thermophysical properties of hard particle fluids, it can also provide various relations describing the radial distribution function.[6,7] Today, SPT is recognized as being part of a more extensive discipline that has come to be known as statistical geometry.[8−10]

A remarkable number of exact relations that bound the properties of hard particle systems can be obtained within SPT. These relations are all derived via straightforward physical and geometric arguments. Therein lies the attractiveness, as well as the effectiveness, of the method. Important and useful insights into the behavior of hard particle systems are readily attained with SPT. Yet, the accuracy of its predictions of various properties of the hard sphere fluid, such as the pressure and excess chemical potential, has not been as high as other more recently developed equations of state.

In the original work, five exact conditions describing the form of the central function *G* (discussed in detail in the next section) were derived. Only three conditions, however, were utilized to determine *G*. Later, Mandell and Reiss[11] applied all five conditions, yielding a much improved equation of state. Despite the number of exact relations that can be employed, the accuracy of these SPT equations of state is limited, particularly at high densities. In the meantime, other equations of state, mostly empirical or semiempirical in nature, have been developed and have surpassed the SPT results.

Unfortunately, no improvements to SPT have been made since the work of Mandell and Reiss. (This is in reference to the accuracy of the equation of state predictions only; other important advances, such as the derivation of various surface thermodynamic relations, have been made.[6]) Nevertheless, SPT still remains an attractive approach because it is well suited to the study of hard particle fluids. With all five of the original exact relations having already been employed, any improvements to the theory must clearly begin with the introduction of new conditions.

With that in mind, we present two new formally exact conditions that further constrain the form of the function *G*. The application of these new relations yields markedly improved predictions of the pressure and excess chemical potential of the hard sphere fluid. The use of these two new conditions requires that various derivatives of *G* be related to the slope and curvature of the hard sphere radial distribution function at contact, $g'(\sigma^+)$ and $g''(\sigma^+)$, respectively. The manipulation of an exact SPT integral equation provides the needed connection between *G* and $g'(\sigma^+)$ and $g''(\sigma^+)$, although additional terms, related to the three-particle correlation function, appear. Because these terms are not known in general, we present a highly accurate approximation to a specific form of the three-particle correlation function also obtained within the framework of SPT. In the end, all relations and corresponding approximations are incorporated into SPT in a self-consistent manner. The two new SPT equations of state are in good agreement with simulation and other literature predictions, further demonstrating the effectiveness of SPT.

The paper is organized as follows. In section 2, we outline the key concepts of SPT and discuss the five previously derived exact relations for the function *G*. In section 3, we present two new formally exact conditions that further restrict the form of

† Part of the special issue "Frank H. Stillinger Festschrift".

* Corresponding author. E-mail: dscorti@ecn.purdue.edu.

10.1021/jp040398b CCC: $27.50
Published on Web 10/21/2004

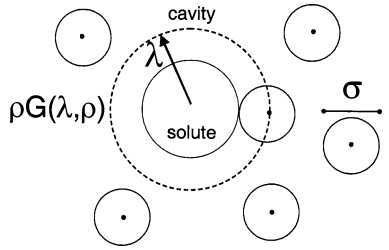

Figure 1. Illustration of the interaction between a cavity of radius λ and spherical hard particles of diameter σ. The centers of the particles are excluded from the dashed volume of the cavity. The solid sphere inside the cavity is the equivalent hard sphere solute of radius $\lambda - \sigma/2$. The local density of hard particle centers in contact with the cavity surface is denoted by $\rho G(\lambda, \rho)$.

G. We then introduce, in section 4, a SPT integral equation that provides the needed connections between the derivatives of the hard sphere radial distribution function and certain derivatives of G. Because some of the functions ultimately appearing in section 4 are not known in general, we discuss in section 5 geometrically and physically based approximations for these terms. In section 6, the details of the simulation methods used to verify our new SPT predictions are presented. Section 7 contains the comparisons of the hard sphere fluid properties as predicted by the new formulations of SPT, using either six or seven conditions, and other equations of state and molecular simulation. We conclude with a final discussion in section 8.

2. Overview of Scaled Particle Theory

Consider a hard sphere fluid at a temperature T comprised of N identical hard particles of diameter σ placed within a macroscopic volume V. Among the particles there is also a spherical cavity of radius λ that, by definition, contains no particle centers (Figure 1). The local density of particle centers in contact with the surface of the cavity is denoted by $\rho G(\lambda,\rho)$, where ρ is the bulk number density N/V. $G(\lambda,\rho)$ is a function of both the cavity radius and the fluid density and is the central function of SPT.[1] Although the precise form of G is not known, various exact relations describing certain properties of G can be generated.

The differential of the reversible work, $W(\lambda)$, required to change the radius λ of the cavity is given by[1]

$$\mathrm{d}W(\lambda) = \rho G(\lambda, \rho) kT 4\pi\lambda^2 \,\mathrm{d}\lambda \tag{1}$$

where k is the Boltzmann constant. G is also connected to the probability that a cavity can be successfully inserted into the volume V (such that the cavity contains no particle centers). This probability, denoted by $p_0(\lambda)$, is related to the function G by the following expression[1]

$$p_0(\lambda) = \exp[-\int_0^\lambda 4\pi r^2 \rho G(r, \rho)\,\mathrm{d}r] = \exp\left(-\frac{W(\lambda)}{kT}\right) \tag{2}$$

For $\lambda = 0$, the above integral vanishes, giving the probability of inserting a cavity of zero radius, $p_0(0)$, a value of unity, consistent with our intuition. In addition, $p_0(\lambda)$ is known exactly for $\lambda \le \sigma/2$, being equal to $1-4\pi\rho\lambda^3/3$ in this range,[1] indicating that

$$G(\lambda, \rho) = \frac{1}{1 - \frac{4\pi\rho\lambda^3}{3}} \tag{3}$$

As discussed in more detail in the Supporting Information, a formally exact relation can be written for $p_0(\lambda)$ in terms of the various hard particle correlation functions. Information about the derivatives of $p_0(\lambda)$ at, for example, $\lambda = \sigma/2$, can be obtained. Consequently, exact expressions for the derivatives of G can be found by repeatedly differentiating eq 2. For example, G and its first derivative, G', are continuous at $\lambda = \sigma/2$ and are equal to[1]

$$G\left(\frac{1}{2}, \eta\right) = (1 - \eta)^{-1} \tag{4}$$

$$G'\left(\frac{1}{2}, \eta\right) = 6\eta(1 - \eta)^{-2} \tag{5}$$

where, for simplicity, we now make use of the dimensionless quantities $\lambda = \lambda/\sigma$ and the packing fraction $\eta = \pi\rho\sigma^3/6$. The second derivative of G, or G'', is, however, discontinuous across $\lambda = 1/2$, in which[1]

$$G''\left(\frac{1}{2} + \epsilon, \eta\right) = \frac{24\eta}{(1 - \eta)}\left[\frac{1 + 2\eta}{(1 - \eta)^2} - 2G(1, \eta)\right] \tag{6}$$

with $\epsilon \to 0$. We note that the discontinuity, represented by the second term on the right side of eq 6, is proportional to $G(1, \eta)$.

Two other conditions that limit the form of G can also be obtained. Because a cavity of radius $\lambda = 1$ is equivalent to another hard particle, $G(1, \eta)$ is therefore equal to the pair correlation function between two hard particles in contact, that is, $G(1, \eta) = g(1^+)$. Hence, the pressure, P, of the hard sphere fluid can be written as[1]

$$\frac{P}{\rho kT} = 1 + 4\eta G(1, \eta) \tag{7}$$

Given that a cavity also becomes equivalent to a hard wall as $\lambda \to \infty$, we have that $P = \rho kTG(\infty,\eta)$. Combining those two expressions yields a fourth exact condition in which[1]

$$G(\infty, \eta) = 1 + 4\eta G(1, \eta) \tag{8}$$

Furthermore, the reversible work required to grow a cavity of radius $\lambda = 1$ is equal to the reversible work required to add another hard particle into the fluid. Thus, $W(1)$ is related to the excess chemical potential of the hard sphere fluid, $\mu^{ex} = \mu - \mu^{id}$, where μ^{id} is the chemical potential of an ideal gas at the same temperature and density, via[1]

$$W(1) = \mu^{ex} = 24\eta kT\int_0^1 r^2 G(r,\eta)\,\mathrm{d}r \tag{9}$$

Substituting eqs 7 and 9 into the following form of the Gibbs−Duhem relationship,

$$P = \int_0^\rho \left(\frac{\delta\mu}{\delta\rho'}\right)_T \mathrm{d}\rho' \tag{10}$$

we obtain the fifth exact condition[1,6]

$$24\eta\int_{\frac{1}{2}}^1 G(r, \eta) r^2\,\mathrm{d}r + \ln(1 - \eta) = 4\int_0^1 G(1, t)\,\mathrm{d}t + 4\eta G(1, \eta) \tag{11}$$

This relation is known as the integral condition of SPT, and it ensures that the resultant form of G is thermodynamically consistent.

To use these five exact relations, a form of $G(\lambda, \eta)$ for $\lambda > {}^1/_2$ must be proposed. Although G is nonanalytic, a smooth function is still chosen to describe G (all of the discontinuities appear in the second and higher-order derivatives[1,6]). For example, from macroscopic thermodynamic considerations, the work of growing a cavity of macroscopic size contains contributions representing both volume work, λ^3, surface work, λ^2, and lower-order corrections. The connection between W and G in eq 1 suggests that G can be well represented, even down to microscopic sizes of $\lambda \approx {}^1/_2$, by a Laurent series[6,11]

$$G(\lambda, \eta) = \sum_{n=0}^{N} G_n(\eta)\lambda^{-n} \tag{12}$$

where the coefficients, G_n, are only functions of η and can be determined by using the various exact conditions of G. In the limit as $\lambda \rightarrow \infty$, the series gives the result of $G(\infty, \eta) = G_0(\eta) = P/\rho kT$. Traditionally, eq 2 has been the assumed form of G. Stillinger and Cotter[12] rigorously showed for $N \geq 3$ that $G_3 = 0$, providing another constraint on the form G (although this condition is contingent upon the choice of the Laurent series to describe G).

In the original SPT paper,[1] only three exact conditions, the continuity of G, and its first derivative, eqs 4 and 5, together with eq 8, were applied to the Laurent series with $N = 2$. The result was the following analytical equation of state

$$\frac{P}{\rho kT} = \frac{1 + \eta + \eta^2}{(1 - \eta)^3} \tag{13}$$

which is identical to the Percus−Yevick equation of state.[45] Equation 12, hereafter referred to as SPT_3, compares well with simulation data for low to moderate packing fractions but deviates above the simulation results at high packing fraction. Later, Mandell and Reiss[11] applied all five exact conditions (eqs 4−6, 8, and 11) with $N = 5$ (along with $G_3 = 0$) to obtain an integral equation for the pressure of the hard sphere fluid. Although the results of ref 11, hereafter referred to as SPT_5, are an improvement over SPT_3, SPT_5 still deviates from simulation values (this time below) at packing fractions close to the freezing transition ($\eta_{freeze} \approx 0.494$[13]). Unfortunately, SPT_5 is not as accurate as other semiempirical equations of state, such as those developed by Carnahan−Starling[14] and Sanchez,[15] despite the fair amount of exact information provided by the framework of SPT. Five conditions, in conjunction with the reasonable choice of a Laurent series to describe G, are still not sufficient to provide an accurate representation of G and, in turn, the hard sphere equation of state at high packing fractions.

SPT, however, is an appealing theoretical approach, primarily because of the large number of exact relations that can be derived in a straightforward manner. Many results in SPT are based on simple geometric arguments and have yielded important physical insights into the properties of hard particle fluids. Although no further improvements to SPT have been made since the work of Mandell and Reiss,[11] whether any additional refinements can be made to SPT remains an open question. Of course, additional conditions on G, besides the five already used, would need to be generated.

One may suppose that improvements to SPT could be obtained if some additional information about G, or its derivatives, at some cavity radius beyond $\lambda = {}^1/_2$ were incorporated into the theory. For example, a discontinuity in the fourth derivative of G appears at $\lambda = 1/\sqrt{3}$, which corresponds to the smallest radius for which three hard particles could fit inside the cavity. This discontinuity, however, is proportional to the three particle correlation function,[1] therefore, it does not appear to provide another useful condition (in general, the discontinuities that appear in the higher-order derivatives of G are related to the higher-order particle correlation functions[1,6]). The number of useful relations describing G appears to remain at five.

Yet, we derive in the next section, two new and formally exact conditions that provide additional constraints on the form of G. In particular, these new relations generate additional information about G and its first two derivatives at $\lambda = 1$. These new conditions, however, cannot be incorporated into SPT in an exact manner. Nevertheless, we are still able to utilize them through the introduction of highly accurate approximations (also obtained within the framework of SPT in Section 5). In the end, these new conditions lead to an improved determination of both G and the properties of the hard sphere fluid at high packing fractions.

3. Two Additional Exact Relations for $G(\lambda,\eta)$

Surprisingly, additional useful conditions can still be obtained if more derivatives of G (beyond the second) are evaluated about $\lambda = {}^1/_2$. Despite appearing to be a simple mathematical exercise, continued differentiation of G at $\lambda = {}^1/_2$ leads to formally exact expressions that can be ultimately exploited.

Let us begin with eq 2, which when differentiated once with respect to λ can be rewritten in the following way[1]

$$4\pi\lambda^2\rho G(\lambda, \eta) = \frac{-p_0'(\lambda)}{p_0(\lambda)} \tag{14}$$

In general, the ith derivative of G can be related to $(i + 1)$ (and lower) derivatives of p_0. As shown in ref 1, the continuity of both G and its first derivative at $\lambda = {}^1/_2$ (eq 4 and 5), as well as the form of the discontinuity of the second derivative of G at this same point (eq 6), can be established through eq 14. The details are provided in the Supporting Information.

We now proceed one step further and evaluate the fourth derivative of p_0, denoted by $p_0^{(4)}$. As shown in the Supporting Information, $p_0^{(4)}$ in the range of ${}^1/_2 \leq \lambda < 1/\sqrt{3}$ is equal to

$$p_0^{(4)}(\lambda) = \rho^2 g(2\lambda)320\pi^2\lambda^2 + \rho^2 g'(2\lambda)128\pi^2\lambda^3 \tag{15}$$

which, when $\lambda = {}^1/_2 + \epsilon$ (as $\epsilon \rightarrow 0$), can be simplified to

$$p_0^{(4)}\left(\frac{1}{2} + \epsilon\right) = 36\eta^2[80G(1, \eta) + 16g'(1^+)] \tag{16}$$

Because the third derivative of G, or G''', is related to $p_0^{(4)}$, we find at the same value of λ that

$$G'''\left(\frac{1}{2} + \epsilon, \eta\right) = \frac{48\eta}{(1 - \eta)}\left[\frac{1 + 16\eta + 10\eta^2}{(1 - \eta)^3} + \frac{2(1 - 13\eta)}{(1 - \eta)}G(1, \eta) - 2g'(1^+)\right] \tag{17}$$

Like G'', G''' is not continuous at $\lambda = {}^1/_2$, the size of the discontinuity being given by the last two terms of the above expression.

Equation 17 is formally exact, although its usefulness appears to be limited due to the appearance of the slope of the radial distribution function at contact, $g'(1^+)$. SPT already provides a direct connection between $g(1^+)$ and $G(1, \eta)$ (eq 8). Whether a connection also exists between $g'(1^+)$ and $G'(1, \eta)$ is not known

as of yet because these two derivatives describe different phenomena. $G'(1, \eta)$ is related to the change in the local density at the cavity surface with the change in the cavity radius. $g'(1^+)$ is related to the change in the local density of hard spheres about another hard sphere fixed at the origin with a change in the distance from the origin. Although in light of these descriptions, one may suspect that some connection does exist. If this connection between $G'(1, \eta)$ and $g'(1^+)$ could be found, then eq 17 would provide a sixth condition that could be used to restrict further the shape of G. In particular, the combination of eq 16 and a relation between $g'(1^+)$ and $G'(1, \eta)$ would yield a condition on the slope of G at the all-important radius of $\lambda = 1$ (so far, the slope has only been restricted at $\lambda = {}^1/_2$). Consequently, eq 17 may lead to an improved equation of state. A formally exact expression that provides the needed connection between $g'(1^+)$ and $G'(1, \eta)$ is derived, still within the framework of SPT, in the next section.

Equation 17 is not strictly new, having been given, without derivation, in refs 1 and 11. In ref 1, it is presented, using slightly different nomenclature, as a route toward the determination of the radial distribution function past its contact value. In ref 11, molecular simulation results are compared with the values of $g'(1^+)$ obtained from eq 17 utilizing the current version of SPT, or SPT_5. Yet, to our knowledge, eq 17 has not been previously applied as another self-consistent condition on G. We discuss this new application of eq 17 in more detail in sections 5 and 7.

Another potentially useful restriction on the form of G can be obtained in a similar manner, by now evaluating the fourth derivative of G. As shown in the Supporting Information, the fifth derivative of p_0 in the range of ${}^1/_2 \le \lambda < 1/\sqrt{3}$ is given by

$$p_0^{(5)}(\lambda) = \rho^2 g''(2\lambda)256\pi^2\lambda^3 + \rho^2 g'(2\lambda)1024\pi^2\lambda^2 + \rho^2 g(2\lambda)640\pi^2\lambda \quad (18)$$

which, at $\lambda = {}^1/_2 + \epsilon$ (as $\epsilon \to 0$), is equal to

$$p_0^{(5)}\left(\frac{1}{2} + \epsilon\right) = 36\eta^2[32g''(1^+) + 256g'(1^+) + 320G(1, \eta)] \quad (19)$$

The above relation now includes both the slope and the curvature of the radial distribution function at contact, $g'(1^+)$ and $g''(1^+)$, respectively. Hence, the fourth derivative of G at the same value of λ, a seventh formally exact condition, is then

$$G^{(4)}\left(\frac{1}{2} + \epsilon, \eta\right) = \frac{192\eta}{(1-\eta)}\left[\frac{6\eta(5 + 17\eta + 5\eta^2)}{(1-\eta)^4} - \frac{3(2 + 9\eta + 49\eta^2)}{(1-\eta)^2}G(1, \eta) - \frac{15\eta}{(1-\eta)}g'(1^+) - g''(1^+)\right] \quad (20)$$

The above connection between $G^{(4)}$ and $g'(1^+)$ and $g''(1^+)$ may give rise to a new condition that prescribes a value to the curvature of G at $\lambda = 1$. The application of both eqs 16 and 19, if possible, along with eq 8, would provide three (two of which are new) restrictions on the form of G at the crucial cavity radius of $\lambda = 1$.

Although formally exact, eqs 17 and 20 are of limited value unless the derivatives of $g(1^+)$ can be related to the function G. In the next section, we present two formally exact expressions, still obtained using SPT, that relate $g'(1^+)$ to $G'(1, \eta)$ and $g''(1^+)$ to $G''(1, \eta)$. The use of these relations does require, however, that particular terms be evaluated approximately. We also discuss, in section 5, physically based approximations to these terms, which, when applied, yield markedly improved predictions compared to SPT_3 and SPT_5.

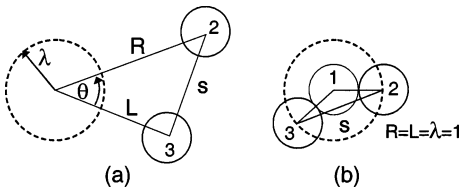

Figure 2. (a) Diagram of the three particles and distances that are involved in eqs 23 and 24. The dashed sphere is the cavity, and the other two solid spheres are particles 2 and 3. In this picture, particle 3 is the nearest neighbor. (b) Specific case when the cavity is equivalent to another hard particle (noted by the inner solid sphere 1 and is in contact with both particles 2 and 3. s denotes the distance between particles 2 and 3.

4. SPT Integral Equation: Derivatives of $g(r)$ at Contact

Before eq 17 and 20 can be fully incorporated into SPT, both $g'(1^+)$ and $g''(1^+)$ must first be related to G and its derivatives. In this section, we derive formally exact expressions that connect G to $g'(1^+)$ and $g''(1^+)$. These new relations are also obtained within the framework of SPT through the use of an SPT integral equation developed by Reiss et al.[16] (an earlier version of this integral equation was first obtained by Reiss and Casberg[7]).

4.1 SPT Integral Equation. Let us consider a cavity of radius λ that is present within the hard particle fluid. The cavity generates an inhomogeneity in the fluid, in which some (spherically symmetric) nonuniform density profile develops about the cavity surface. The local density of particles at a distance R from the cavity center will be denoted by $\rho g(\lambda, R)$, where $g(\lambda, R)$ is the cavity−particle correlation function. Because no particle centers can lie inside the cavity, $g(\lambda, R) = 0$ for $\lambda < R$. Also, because a cavity becomes equivalent to another hard particle when $\lambda = 1$, $g(1, R) = g(r)$, where $g(r)$ is the radial distribution function of the hard particle fluid.

As shown by Reiss et al.,[16] $\rho g(\lambda, R)$ can be expressed as the sum of two separate terms. For example, consider the local density of spheres within $d\vec{R}$ located at a position $\vec{R}$ from the center of the cavity. The probability density that a particle, say particle 2, is found at $\vec{R}$ is given by $\rho g(\lambda, R)\, d\vec{R}$, where R is the magnitude of $\vec{R}$. Now, particle 2 can either be the nearest neighbor of the cavity (i.e., that particle closest to the cavity) or, if it is not the nearest neighbor, then some other particle, say particle 3, must be the nearest neighbor (Figure 2a). Therefore, $\rho g(\lambda, R)\, d\vec{R}$ is comprised of two separate contributions: the probability that particle 2 at $d\vec{R}$ is the nearest neighbor, and the probability that particle 2 is located at $d\vec{R}$ given that particle 3 is the nearest neighbor. In other words,[16]

$$\rho g(\lambda, R)\, d\vec{R} = \beta(\lambda, R)\, d\vec{R} + [\rho \int_\lambda^R \beta(\lambda, L) g^{[3]}(\vec{L}, \vec{R})\, d\vec{L}]\, d\vec{R} \quad (21)$$

where $\beta(\lambda, R)$ is the nearest-neighbor probability density distribution. $\rho g^{[3]}(\vec{L}, \vec{R})$ is the conditional probability density of a particle being located at $d\vec{R}$ given a cavity of radius λ at the origin and the nearest neighbor of the cavity being within $d\vec{L}$ at a distance L from the center of the cavity. The limits of the integral ensure that particle 3 remains the nearest neighbor of the cavity while still being excluded from the cavity, that is, $\lambda \le |\vec{L}| \le |\vec{R}|$. In general, $g^{[3]}(\vec{L}, \vec{R})$ is not known, although $\beta(\lambda, R)$ can be expressed in terms of G, where[16]

$$\beta(\lambda, R) = \rho G(R) \exp[-\int_\lambda^R \rho G(r) 4\pi r^2\, dr] \quad (22)$$

in which we have dropped the explicit reference to density in the function G. Because the cavity has already excluded particle centers within a radius of λ, the probability that the remaining volume up to a radius R is devoid of particle centers is the negative of the exponential of the reversible work required to grow the cavity from λ to R. When multiplied by the particle density at the surface of the cavity of radius R, this quantity yields the nearest-neighbor probability density distribution.

Because the hard particle fluid is isotropic, $g^{[3]}$ can be expressed in terms of relative positions in which $g^{[3]} = g^{[3]}(L,\theta, R)$ (where θ is the angle that separates $\vec{R}$ and $\vec{L}$, Figure 2a). We now introduce $\bar{g}$, the value of $g^{[3]}$ averaged over a sphere of radius L,[7,17] in which

$$\bar{g}(L, R) = \frac{1}{4\pi}\int_0^{2\pi} d\phi \int_0^{\pi} g^{[3]}(L, \theta, R) \sin\theta \, d\theta \qquad (23)$$

Substituting $\bar{g}$ into eq 20 results in a more convenient expression[16]

$$\rho g(\lambda, R) = \beta(\lambda, R) + \rho \int_{\lambda}^{R} \beta(\lambda, L)\, \bar{g}(L, R) 4\pi L^2 \, dL \quad (24)$$

Although the above is exact, $\bar{g}(L, R)$ is not known in general. $\bar{g}(L, R)$ is, however, known exactly for certain values of λ and R. For example, when $\lambda \leq {}^1/_2$, where the exclusion sphere of particle 3 completely covers the cavity, $\bar{g}(L, R) = g(1,|\vec{L} - \vec{R}|)$. For additional details concerning the properties of $\bar{g}(L, R)$, the reader is referred to refs 7 and 17.

The radial distribution function, $g(r)$, of the hard particle fluid can be written as a specific case of the cavity−particle correlation function. When the cavity radius, λ, is equal to 1, the cavity is equivalent to a particle, so $g(1, R) = g(r)$, and

$$g(1, R) = G(R) \exp\left[-\int_1^R \rho G(r) 4\pi r^2 \, dr\right] + \int_1^R \beta(1, L)\, \bar{g}(L, R) 4\pi L^2 \, dL \quad (25)$$

Using the above equation, one can derive the needed connections between the various derivatives of $g(r)$ and G.

4.2 Slope and Curvature of *g*(*r*) at Contact. We begin by differentiating eq 24 with respect to R

$$\frac{dg(1, R)}{dR} = \left(\frac{dG(R)}{dR} - \rho[G(R)]^2 4\pi R^2\right) \exp\left[-\int_1^R \rho G(r) 4\pi r^2 \, dr\right] + \int_1^R \beta(1, L) \frac{d\bar{g}(L, R)}{dR} 4\pi L^2 \, dL + \rho\beta(1, R)\, \bar{g}(R, R) 4\pi R^2 \quad (26)$$

Setting $R = 1$ results in a reduction of terms and a final result of

$$\left(\frac{dg(1, R)}{dR}\right)_{R=1} = g'(1^+) = G'(1) - 24\eta[G(1)]^2\left[1 - \frac{\bar{g}(1, 1)}{G(1)}\right] \quad (27)$$

This expression provides an exact connection between $g'(1^+)$ and $G'(1)$. What now appears, however, is the new term, $\bar{g}(1, 1)$, or the average value of the three particle distribution function (the cavity is now equivalent to another particle) with two particles in contact while the third particle changes position but remains in rolling contact with at least one of the other two. (See Figure 2b, which shows the specific case of eq 24 for $R = 1$.) In the next section, we discuss an accurate approximation to $\bar{g}(1, 1)$ that can also be derived within SPT. Before determining this approximation, we first consider the second derivative of $g(r)$.

Differentiating eq 25 with respect to R, and then letting $R = 1$, results in

$$g''(1^+) = G''(1) - 24\eta G'(1)\, G(1)\left[3 - \frac{\bar{g}(1, 1)}{G(1)}\right] + (576\eta^2[G(1)]^3 - 48\eta[G(1)]^2)\left[1 - \frac{\bar{g}(1, 1)}{G(1)}\right] + 24\eta G(1)\left[\left(\frac{d\bar{g}(L, R)}{dR}\right)_{L=R} + \left(\frac{d\bar{g}(R, R)}{dR}\right)\right]_{R=1} \quad (28)$$

The above equation yields the needed relationship between $g''(1^+)$ and $G''(1)$ (as well as $G'(1)$ and $G(1)$), although the unknown quantities $\bar{g}(1, 1)$ and its two derivatives also appear. The number of terms in eq 28 substantially increases as compared to that in the expression for $g'(1^+)$ in eq 27. The last two terms on the right side of eq 28 are the derivatives of $\bar{g}$ evaluated in two different ways. The first derivative, $d\bar{g}(L, R)/dR$, corresponds to the change in $\bar{g}$ with respect to a change in the distance to particle 2 when the position of the nearest neighbor, particle 3, is fixed (L = constant). The second derivative, $d\bar{g}(R, R)/dR$, considers the change in $\bar{g}$ when the distances to both particle 2 and particle 3, set to be equal ($L = R$), are varied.

Equations 27 and 28 reveal that the slope and curvature of $g(1^+)$ are related to the slope and curvature of $G(1)$. Yet, these connections can only be exploited if the function $\bar{g}(L, R)$, or $\bar{g}(1, 1)$, in particular, can be determined (or accurately approximated). Only then can the sixth and seventh conditions on G, eqs 17 and 20, finally be used.

5. Approximate Expression for $\bar{g}(L, R)$ and Its Derivatives

As stated previously, the application of eqs 17 and 20 requires, via eqs 27 and 28, knowledge of the three particle correlation function $\bar{g}(L, R)$. Because $\bar{g}(L, R)$ is not known in general, a reasonably accurate approximation to $\bar{g}(L, R)$ is needed. Yet, generating an accurate approximation to $\bar{g}(L, R)$ is a difficult task given that $\bar{g}(L, R)$ is presumably a complicated function. Fortunately, our task is made easier because we require only $\bar{g}(1, 1)$ and two of its first derivatives. In addition, we should attempt to obtain an expression for $\bar{g}(1, 1)$ completely within the framework of SPT itself. Hence, all expressions used for the determination of G and the corresponding hard particle properties follow from SPT, thereby generating a self-consistent theoretical approach.

5.1 Determination of $\bar{g}(1, 1)$. $\bar{g}(L, R)$ can be more conveniently expressed through the use of bipolar coordinates as[7]

$$\bar{g}(L, R) = \frac{1}{2LR}\int_{R-L}^{R+L} g^{[3]}(R, s, L) s \, ds \qquad (29)$$

where s now represents the distance between the centers of particles 2 and 3, as shown in Figures 2b and 3. For the specific case of $\bar{g}(1, 1)$, we have that

$$\bar{g}(1, 1) = \frac{1}{2}\int_1^2 g^{[3]}(1, s, 1) s \, ds \qquad (30)$$

where $g^{[3]}(1, s, 1)$ is the conditional probability for three hard particles (all of diameter 1) in rolling contact. The lower limit of the integral in eq 30, although strictly zero, is set at unity because the hard sphere potential forbids any configurations for

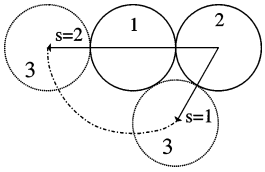

Figure 3. Two limits of integration of eq 30, represented by the two positions of particle 3 (dashed sphere). Note that particles 1 and 2 remain in contact throughout the change in position of particle 3. Additionally, particle 3 remains in contact with particle 1 throughout its motion. The dot−dashed arc represents the path of the center of particle 3 over which $g^{[3]}$ is integrated in eq 30. The value of $g^{[3]}(1, s, 1)$ varies as particle 3 changes position.

$s < 1$. This is illustrated in Figure 3, where particles 1 and 2 remain in contact with each other while particle 3, also remaining in contact with particle 1, moves between $s = 1$ (all three particles in contact) and $s = 2$ (a linear arrangement)

The values of $g^{[3]}(1, s, 1)$ for different distances s can be related to one another via Widom's inverse potential distribution theory[18] (a special form of which, based on fluctuation theory, was introduced earlier in SPT[1]). If $W(s)$ represents the reversible work required to insert, or grow, particle 3 at a distance s from particle 2 while both 2 and 3 are still in contact with particle 1, then the ratio of $g^{[3]}(1, s, 1)$ to $g^{[3]}(1, s_o, 1)$, where s_o is some chosen reference distance of separation between 2 and 3, is explicitly given by[17]

$$\frac{g^{[3]}(1, s, 1)}{g^{[3]}(1, s_o, 1)} = \exp\left[-\left(\frac{W(s) - W(s_o)}{kT}\right)\right] \qquad (31)$$

If a reference value for $g^{[3]}$ is known, then the determination of $W(s)$ provides the appropriate value of $g^{[3]}(1, s, 1)$.

The choice of a reference point for $g^{[3]}$ follows from a simple physical argument. Consider the linear arrangement of the spheres in which $s = 2$ (Figure 3). In this configuration, particle 1 prevents any direct interaction between particles 2 and 3. As a first approximation, it is reasonable to assume that in this linear arrangement particle 2 does not "feel" the presence of particle 3. Thus, $g^{[3]}$ becomes equivalent to the contact value of the radial distribution between particles 1 and 2. In other words, we let $g^{[3]}(1, s = 2, 1) = g(1^+) = G(1)$. Because particles 2 and 3 still interact indirectly, this assumption is not strictly correct. In one dimension (hard rod fluid), however, this approximation is exact, and it is also exact in higher dimensions in the limit as $\rho \to 0$. In addition, as discussed later, a numerical solution of $g^{[3]}$ (via the PY closure; shown to be in agreement with a simulation[20]) performed by Attard and Stell[19] does indicate that $g^{[3]}(1, s = 2, 1) \approx g(1^+)$ over a broad range of fluid densities.

Now that a reference state has been selected, the next step is to obtain an expression for $W(s)$. The reversible work of growing the particle, or equivalent-sized cavity, can be estimated using the SPT formalism. The reversible work of growing a cavity that overlaps another surface, a hard wall, for example, can be expressed as[21]

$$W = P\Delta V + \Delta(\gamma_r A) + \cdots \qquad (32)$$

where P is the bulk pressure of the fluid and ΔV and ΔA are the volume and surface area, respectively, of a cavity that does not overlap the exclusion zone of the wall and γ_r is the size-dependent surface tension of the cavity. Additional terms, such as the line tension between the hard wall−cavity−fluid contact line, contribute as well.[21] This work expression also applies to the determination of $W(s)$, where $\Delta V(s)$ now refers to the volume

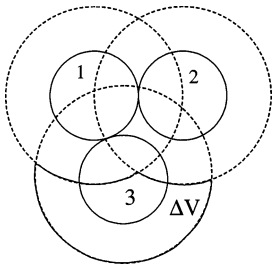

Figure 4. Illustration of the partial exclusion volume of particle 3, ΔV (outlined region), that does not overlap the exclusion volumes of particles 1 and 2. As the distance between particles 2 and 3 changes (while particles 1 and 3 remain in contact), ΔV changes as well, becoming smaller as all three particles come into contact.

created by the exclusion sphere of particle 3 that does not overlap the exclusion volumes of either particle 1 or 2 (Figure 4; each hard particle is surrounded by a exclusion sphere with a radius equal to the diameter of a hard particle and denotes the region in which the center of another hard particle cannot enter).

One may consider using only the $P\Delta V$ term in eq 32. The resulting expression significantly overestimates W because the negative contribution from γ_r ($\gamma_r \leq 0$) is missing. To avoid calculating surface areas, we estimated $W(s)$ using the following approximation[17]

$$W(s) \approx \rho kT\Delta V(s) \qquad (33)$$

where the ideal gas pressure (based on the bulk density ρ) has been employed in place of the hard sphere pressure. This ideal gas approximation (first utilized by Asakura−Oosawa[22]) is convenient to work with and still captures some of the cancellation between the positive hard sphere pressure term and the negative surface tension term. Still, eq 33 appears, at first sight, to be a less than appropriate starting point for generating predictions of $g^{[3]}(1, s, 1)$ via eq 31. Note that we are ultimately interested in generating an accurate approximation to $\bar{g}(1, 1)$ and not necessarily $g^{[3]}$. If the average value of $g^{[3]}$,that is, $\bar{g}(1, 1)$, is well represented by eq 32, then we are justified in using the ideal gas approximation. As we discuss later in this section, molecular simulation results validate the use of eq 33 for obtaining estimates of $\bar{g}(1, 1)$.

We now substitute both our choice of $g^{[3]}(1, s = 2, 1) = g(1^+) = G(1)$ and eq 33 into eq 31. Consequently, we obtain the following approximation for $g^{[3]}(1, s, 1)$

$$g^{[3]}(1, s, 1) = G(1)\exp\left[\frac{6\eta(\Delta V_{ref} - \Delta V(s))}{\pi}\right] \qquad (34)$$

where ΔV_{ref} is the volume of the exclusion sphere of particle 3 that does not overlap the exclusion spheres of particles 1 and 2 when all three spheres are collinear ($s = 2$). This reference volume is exactly known and is equal to $\Delta V_{ref} = 11\pi/12$. $\Delta V(s)$ can also be determined exactly because the volume of overlap between three spheres is known.[23]

Using eq 30, the resultant expression for $\bar{g}(1, 1)$ becomes

$$\bar{g}(1, 1) = \frac{G(1)}{2}\int_1^2 \exp\left[\frac{6\eta(\Delta V_{ref} - \Delta V(s))}{\pi}\right] s\, ds \qquad (35)$$

in which $G(1)$, not a function of s, has been moved in front of the integral. The exponent in the integrand represents the change in the excluded volume associated with the "grown" particle as it interacts with the exclusion spheres of the other two spheres. Equation 35 does not integrate analytically and must be

evaluated numerically due to the complexity of the geometric quantities needed to determine $\Delta V(s)$. The above integral, however, can be immediately evaluated over a limited range of s. For $\sqrt{3} \leq s \leq 2$, the exclusion sphere of particle 3 only overlaps the exclusion sphere of particle 2 within the exclusion sphere of particle 1. Hence, $\Delta V(s) = \Delta V_{\text{ref}}$ over this range, which means that eq 35 can be simplified to

$$\frac{\bar{g}(1,1)}{G(1)} = \frac{1}{4} + \frac{1}{2}\int_1^{\sqrt{3}} \exp\left[\frac{6\eta(\Delta V_{\text{ref}} - \Delta V(s))}{\pi}\right] s\, ds \quad (36)$$

Overall, the range of numerical integration is small. The exponential term reaches a maximum value when $s = 1$, and in that limit, $\Delta V_{\text{ref}} - \Delta V(1) \approx 0.2028\pi$ or about 15% of the volume of an individual exclusion sphere. Equation 36 also indicates that as $\eta \rightarrow 0$, $\bar{g}(1,1)/G(1) = \bar{g}(1,1)/g(1^+) \rightarrow {}^3/_4$.

At a density of $\rho\sigma^3 = \rho^* = 0.9$, eq 34 predicts that when all three particles are touching ($s = 1$) the value of $g^{[3]}$ is equal to $1.77G(1)(1.77g(1^+))$. Work by Attard and Stell[19] indicates that this prediction of $g^{[3]}$ is around 50% lower than the actual value at that density. This difference does not, however, affect the accuracy of our approximation to $\bar{g}(1,1)$. The integrand in eq 35 is always greater than or equal to unity, indicating that $g^{[3]}(1, s, 1) \geq g(1^+)$. However, the results of ref 19 reveal that $g^{[3]}(1, s, 1)$ oscillates above and below $g(1^+)$ over the full range of s. This does not necessarily invalidate our use of eq 33. Our new conditions on G only require that we generate accurate approximations to $\bar{g}(1,1)$ and not necessarily replicate the detailed structure exhibited by $g^{[3]}(1, s, 1)$.

To check whether eq 36 does provide reasonable values for $\bar{g}(1,1)$, we compared the values of $\bar{g}(1,1)/G(1)$ obtained from a set of Monte Carlo (MC) simulations results that we generated with the predictions of eq 36. (Our simulation methods are described in detail in section 6.) We list in Table 1 the values of $\bar{g}(1,1)/G(1)$ from both the simulation and eq 36. Interestingly, the use of the ideal gas approximation to estimate $W(s)$ leads to highly accurate predictions of $\bar{g}(1,1)$. Although our approximation does not correctly reproduce the full structure of $g^{[3]}$, upon integration (eq 30), the resultant average value, or $\bar{g}(1,1)$, matches the simulation results quite well. Note that in the zero density limit, $\bar{g}(1,1)/G(1) = {}^3/_4$, and at $\eta = 0.49$, $\bar{g}(1,1)/G(1) \approx 0.853$, indicating that $\bar{g}(1,1)/G(1)$ is not a strong function of η.

With our chosen expression for $\bar{g}(1,1)$, we can approximate the slope of the radial distribution at contact by

$$g'(1^+) = G'(1) - 24\eta[G(1)]^2\left(\frac{3}{4} - \frac{1}{2}\int_1^{\sqrt{3}} \exp\left[\frac{6\eta(\Delta V_{\text{ref}} - \Delta V(s))}{\pi}\right] s\, ds\right) \quad (37)$$

The above relation can be used in eq 17 so that we now have a set of six self-consistent conditions on G. The use of eq 37 ultimately serves to constrain not only G at $\lambda = 1$ but also the slope of G at $\lambda = 1$.

5.2 Derivatives of $\bar{g}(1,1)$ Using the Ideal Gas Approximation. Our approximation for $\bar{g}$ also allows us to generate an approximation to $g''(1^+)$ via eq 28. In this case, we also need to evaluate two derivatives of $\bar{g}$ of that appear in eq 28 also using the ideal gas approximation. The full details of the differentiation are provided in the Supporting Information, and we only present the main results in this section.

TABLE 1: Comparison of $\bar{g}(1,1)/G(1)$[a] for Different Packing Fractions as Determined by Monte Carlo (MC) Simulations and as Predicted by Equation 36

	eq 36	MC
η	$\bar{g}(1,1)_{\text{approx}}/G(1)$	$\bar{g}(1,1)/G(1)$
0.052	0.7593	0.7639
0.157	0.7791	0.7792
0.209	0.7896	0.7897
0.262	0.8004	0.8019
0.314	0.8117	0.8122
0.367	0.8234	0.8246
0.419	0.8356	0.8367
0.471	0.8483	0.8512

[a] The ratio of $\bar{g}(1,1)$ to $G(1)$ was not determined directly from simulation but instead was calculated using two separate sets of simulations.

Using the formal definition of $\bar{g}$ in eq 29 along with eq 35, $d\bar{g}(L,R)/dR$, when evaluated at $L = R$ and then with $R = 1$, is given by

$$\left[\left(\frac{d\bar{g}(L,R)}{dR}\right)_{L=R}\right]_{R=1} = G(1) - \bar{g}(1,1) + g'(1^+)\frac{\bar{g}(1,1)}{G(1)} + \frac{G(1)}{2}\int_1^2 \frac{6\eta}{\pi}\left[\left(\frac{d\,(\Delta V_{\text{ref}} - \Delta V(s))_{L,s,R}}{dR}\right)_{L=R}\right]_{R=1} \times \exp\left[\frac{6\eta(\Delta V_{\text{ref}} - \Delta V(s))}{\pi}\right] s\, ds \quad (38)$$

where the subscript "L, s, R" indicates that the derivative of the volumes in the exponent is specific to the choice of L, s, and R. The other derivative in eq 27, $d\bar{g}(R,R)/dR$, is now approximated by

$$\left(\frac{d\bar{g}(R,R)}{dR}\right)_{R=1} = 2G(1) - 2\bar{g}(1,1) + G'(1)\frac{\bar{g}(1,1)}{G(1)} + \frac{G(1)}{2}\int_1^2 \frac{6\eta}{\pi}\left(\frac{d\,(\Delta V_{\text{ref}} - \Delta V(s))_{R,s,R}}{dR}\right)_{R=1} \times \exp\left[\frac{6\eta(\Delta V_{\text{ref}} - \Delta V(s))}{\pi}\right] s\, ds \quad (39)$$

Again, eq 39 contains a derivative of the volume term in the exponent (denoted by the subscript "R, s, R"), whose value will be slightly different than it is in eq 38.

At this point, we can substitute our approximations for $d\bar{g}/dR$ into eqn 28, which results in the following working form of the curvature of the radial distribution function at contact

$$g''(1^+) = G''(1) - 24\eta G'(1)G(1)\left[3 - \frac{\bar{g}(1,1)}{G(1)}\right] + (576\eta^2[G(1)]^3 + 24\eta[G(1)]^2)\left[1 - \frac{\bar{g}(1,1)}{G(1)}\right] + 48\eta G(1)\frac{\bar{g}(1,1)}{G(1)}\left(G'(1) - 12\eta G(1)\left[1 - \frac{\bar{g}(1,1)}{G(1)}\right]\right) + 24\eta[G(1)]^2 \times \int_1^2 \frac{3\eta}{\pi}\left[\frac{d\,(\Delta V_{\text{ref}} - \Delta V(s))_{R,s,R}}{dR} + \left(\frac{d\,(\Delta V_{\text{ref}} - \Delta V(s))_{L,s,R}}{dR}\right)_{L=R}\right]_{R=1} \exp\left[\frac{6\eta(\Delta V_{\text{ref}} - \Delta V(s))}{\pi}\right] s\, ds \quad (40)$$

The numerical value of the integral in eq 40 is fairly small. At the limit of zero density, the integral is identically zero, and at $\eta = 0.49$, the integral is approximately equal to 0.283. The

integral term is multiplied by $[G(1)]^2$, however, so as η increases, it becomes a numerically significant quantity.

6. Simulation Methods

The use of all six and seven conditions within SPT generates new predictions for the hard sphere pressure, the work of cavity formation, $W(\lambda)$ (including the specific case of $\mu^{ex} = W(1)$), the slope and curvature of $g(1^+)$, and the average value of the three-particle correlation function $\bar{g}(1, 1)$. To test the accuracy of these predictions, we compared the SPT estimates with the results of molecular simulation.

First, to calculate a value of $\bar{g}(1, 1)$ from simulation, two fluid particles were held in contact at the center of the simulation box within a constant N, V, T MC simulation. Periodic boundary conditions were applied, and the usual Metropolis algorithm[24] was employed. We used a system size of $N = 500$ particles (counting the two particles held at the origin), and at each packing fraction, 10^7 cycles (where a cycle represents N attempted particle moves) were run after equilibration. The center of each of the two spheres placed in contact was chosen as the origin to determine the local density of hard particles a distance r away. The value of r, however, was calculated using the origin that yielded the minimum value of r. In other words, symmetric, dumbbell-shaped shells of varying sizes (or distances r from either origin) were placed about the two particles in contact, and the local density within each shell was calculated. At the end of the simulation, the local density within each shell at a distance r from either origin was divided by the bulk density and the natural log of this distribution function for small r values was fit to a third-order polynomial. The polynomial function was then extrapolated to contact, or $r \rightarrow 1$, yielding an estimate of the conditional probability density $\bar{g}(1, 1)$.

To determine $g(1^+)$ and its derivatives, we again utilized a standard MC simulation with constant N, V, and T. These simulations were run for at least 4×10^6 cycles, and up to 2×10^7 cycles, with a system size of $N = 1372$ particles. The radial distribution function was determined at each density, and the natural log of the radial distribution function near contact was fit to a third-order polynomial. The contact value, $g(1^+)$, was determined via extrapolation of this fit and was used to calculate the pressure.[24] To calculate $g'(1^+)$, we took the derivative of the third-order fit and extrapolated it to contact. Similarly, we took two derivatives of the polynomial fit to find the value of $g''(1^+)$.

For each of these first two sets of simulations, error bars were estimated by taking averages of the desired quantities within smaller blocks of a fixed number of cycles (the number of cycles comprising a given block ranged from 5×10^5 cycles to 10^6 cycles for the 4×10^6 cycle simulation and the 2×10^7 cycle simulation, respectively). For example, within each block, the near contact portion of the radial distribution function, $g(r)$, was fit to a third-order polynomial. The contact values obtained from these smaller blocks were then used to determine the standard deviation of $g(1^+)$.

Finally, we carried out a number of MC simulations at constant N, P, and T to determine values of $W(\lambda)$ for cavity sizes larger than $\lambda = 1/2$. In a system of $N = 500$, a cavity was held fixed at the center of the simulation box. An additional MC move was performed in which the radius of the cavity was randomly varied by a small amount (all particle centers were excluded from the cavity). Using a self-consistent umbrella sampling method,[24] we added a biasing potential to the MC acceptance criteria for cavity radii changes to enable the cavity to sample a sufficient range of radii within a given range, or window, of allowed radii. The length of each simulation was adjusted so that the calculated biased probability densities (of finding a cavity of radius λ around a given increment) were nearly uniform within the given window of sampled radii. The biasing potential was then used to generate the unbiased probability densities, $p_0(\lambda)$, in which the logarithmic ratio of the unbiased probabilities, $\ln[p_0(\lambda_i)/p_0(\lambda_j)]$, equals the free-energy difference, or reversible work, required to grow a cavity from radius λ_i to radius λ_j. Because $W(\lambda)$ is known exactly for $\lambda \leq 1/2$, the reversible work to grow cavities of larger radii can be found by linking together the results of each window. In this way, we were able to determine $W(\lambda)$ up to values of $\sim 100kT$.

7. New Formulations of $G(\lambda, \eta)$: Six and Seven Conditions

We now consider the incorporation of our two new conditions, eqs 17 and 20, into SPT. The use of the original five conditions plus eq 17 is denoted by SPT_6, and the use of all seven conditions, the original five plus eqs 17 and 20, is labeled as SPT_7.

For clarity, the six conditions that comprise SPT_6 are

$$G(\infty) = 1 + 4\eta G(1) \quad G\left(\frac{1}{2}\right) = (1 - \eta)^{-1}$$

$$G'\left(\frac{1}{2}\right) = 6\eta(1 - \eta)^{-2}$$

$$G''\left(\frac{1}{2}\right) = \frac{24\eta}{(1 - \eta)}\left(\frac{1 + 2\eta}{(1 - \eta)^2} - 2G(1)\right)$$

$$G'''\left(\frac{1}{2}\right) = \frac{48\eta}{(1 - \eta)}\left(\frac{1 + 16\eta + 10\eta^2}{(1 - \eta)^3} + \frac{2(1 - 13\eta)}{(1 - \eta)}G(1) - 2g'(1^+)\right)$$

$$24\eta\int_{\frac{1}{2}}^{1} G(r)r^2\,dr + \ln(1 - \eta) = 4\int_0^{\eta} G(1)\,dt + 4\eta G(1) \quad (41)$$

in which $g'(1^+)$ is exactly given by

$$g'(1^+) = G'(1) - 24\eta[G(1)]^2(1 - \alpha) \quad (42)$$

where $\alpha \equiv \bar{g}(1, 1)/G(1)$ and can be determined numerically using the approximation, eq 36, that was derived in section 5. As done for SPT_3 and SPT_5, we represent $G(\lambda)$ by a Laurent series, eq 2, with $N = 6$, where we also invoke the additional requirement that $G_3(\eta) = 0$.[12] After substituting the Laurent series expansion for $G(\lambda)$ into eqs 41 and 42, one can combine the results and solve for $G_0(\eta)$ (which is also equivalent to the compressibility factor, $Z = P/\rho kT$). After some lengthy algebra, the following integral equation for $G_0(\eta)$ is obtained

$$G_0(\eta) = 1 - \ln[1 - \eta] + A(\eta, G_0) + B(\eta, G_0, \alpha) - C(\eta) - \int_0^{\eta}\frac{G_0(t) - 1}{t}dt \quad (43)$$

where

$$A(\eta, G_0) = G_0(\eta)\left(\frac{768 - 2108\eta + 1229\eta^2 - 30\eta^3}{4(1 - \eta)(224 - 243\eta)}\right)$$

$$B(\eta, G_0, \alpha) = 18\eta\left(\frac{[G_0(\eta)]^2 - \alpha(G_0(\eta) - 1)^2}{(224 - 243\eta)}\right)$$

$$C(\eta) = \frac{768 - 6772\eta + 12305\eta^2 - 9598\eta^3 + 2667\eta^4}{4(1-\eta)^3(224 - 243\eta)} \quad (44)$$

SPT_7 uses all of the conditions for SPT_6, eq 41, but now includes one additional term, in which

$$G^{(4)}\left(\frac{1}{2}\right) = \frac{192\eta}{(1-\eta)}\left[\frac{6\eta(5 + 17\eta + 5\eta^2)}{(1-\eta)^4} - \frac{3(2 + 9\eta + 49\eta^2)}{(1-\eta)^2}G(1) - \frac{15\eta}{(1-\eta)}g'(1^+) - g''(1^+)\right] \quad (45)$$

With one more equation, one more term is needed in the Laurent series ($N = 7$ and $G_3(\eta) = 0$). Again, one can solve for $G_0(\eta)$, and the resulting integral equation is similar to eq 43. The result, however, contains three quantities that must be numerically integrated (α and the two derivatives of $\bar{g}(1, 1)$, see eq 40).

For both SPT_6 and SPT_7, the integral equations were solved via an iterative procedure, which readily converged. All numerical integration was performed using extended Simpson's rule or an equivalent fourth-order method.[25] We now consider the new formulations of SPT, and their subsequent predictions of P, $g'(1^+)$, $g''(1^+)$, μ^{ex} and $W(\lambda)$.

7.1 Pressure of the Hard sphere Fluid. Figure 5 compares the pressure, $P\sigma^3/kT$, of the hard sphere fluid as predicted by the four versions of SPT discussed in this paper with the results of molecular simulation. As hoped, the SPT_6 and SPT_7 are much closer to the simulation values than SPT_3 or SPT_5. In fact, SPT_6 is nearly indistinguishable from the simulation values on the scale of the plot. SPT_7 slightly overestimates the simulation pressure at high packing fractions, but it is still a marked improvement over SPT_3 and SPT_5. Unquestionably, the addition of more constraints on the form of G results in improved pressure predictions. The accuracy of SPT_6 clearly validates our use of eq 35 as an approximation to $\bar{g}(1, 1)$. The lesser accuracy of SPT_7 is presumably due to the use of eqs 38 and 39 to estimate the derivatives of $\bar{g}(1, 1)$, where more detailed knowledge of the structure of $g^{[3]}$ is required to fully capture $g''(1^+)$. Better estimates of the derivatives of $g^{[3]}$ may further improve the accuracy of SPT_7.

Both SPT_6 and SPT_7 also compare favorably to other current equations of state of the hard sphere fluid. To limit the total number of equations of state to consider, we opted to compare our results with only a few of the many available expressions (for a relatively comprehensive list of hard sphere equations of state, most of which are empirical and semiempirical, see refs 26 and 27). In this paper, we consider the following relations: the Carnahan−Starling (CS) equation of state,[14] a simple, semiempirical expression that is still one of the most accurate equations of state, the equation of state formulated by Sanchez (S), which utilizes a 4,3-Padé approximant to replicate the eight known virial coefficients of the hard sphere fluid,[15] and a more recent equation of state derived by Yelash and Kraska (YK)[28] that incorporates the high-density limit (requiring that the pressure diverges to infinity at the limit of the maximum packing fraction). We employ the unsimplified version of YK[28] because accuracy, rather than convenience, is the motivation for our comparison.

In Table 2, we compare the pressure, $P\sigma^3/kT$, obtained from SPT_6 and SPT_7 with the predictions of the CS, S, YK, and SPT_3 equations of state. We also include two sets of simulation results, the MC simulation data generated for this work, labeled MC′, and the recent molecular dynamics (MD) data generated by Kolafa et al.,[29] labeled as MD. Our simulation results are in very good agreement with the highly accurate data of Kolafa et al. Pressures below packing fractions of $\eta = 0.288$ are not shown because the differences between the various equations of state and simulation values are minor (SPT_3 is in agreement with simulation up to $\eta \approx 0.25$). The simulation values are larger than CS predictions but fall below the S and YK values.

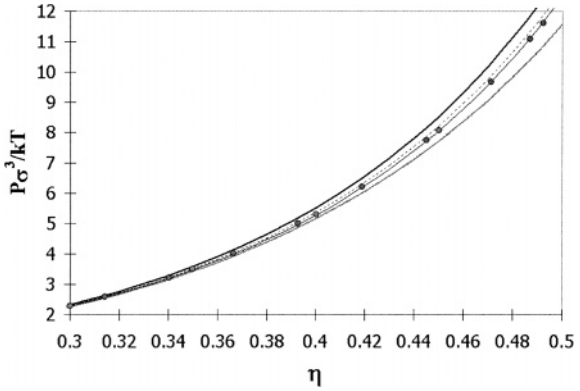

Figure 5. Pressure, $P\sigma^3/kT$, of the hard sphere fluid versus packing fraction, η. The solid symbols represent Monte Carlo simulation values. The thick upper line is the prediction of SPT_3, the thick lower line is SPT_5, the solid middle line is SPT_6, and the dashed line is SPT_7.

Table 2 reveals the marked improvement in the accuracy of SPT that has been gained by the addition of new conditions and the use of an accurate closure to estimate $\bar{g}(1, 1)$ and its derivatives. For $\eta \leq 0.492$ ($\rho^* = 0.94$), SPT_6 predictions deviate by no more than 0.6% from simulation data. SPT_7 consistently overestimates, although slightly, the pressure. Even so, at $\eta = 0.471$, SPT_7 only exceeds the simulation results by about 2%. The increased accuracy of SPT is also apparent when SPT_6 and SPT_7 are compared to SPT_3. For example, at $\eta = 0.487$, SPT_3 deviates from simulation by about 7%, SPT_6 by about 0.3%, and SPT_7 by about 2%. The use of new conditions on G has finally yielded SPT predictions, in particular, SPT_6, that are at least comparable to, if not better than, several widely used empirical and semiempirical equations of state.

Additional values of the hard sphere pressure at $\eta \geq 0.25$ are presented in Table 3 along with one other equation of state and another set of simulation data. Also included are the predictions of the equation of state of Labik et al. (L).[30,31] Their equation of state incorporates, like SPT, information on the pair and triplet correlation functions and, also like SPT, is a purely theoretical approach. Results from simulations performed for this work are again labeled MC, whereas the fit of literature simulation data generated by Erphenbeck and Wood (EW)[32] is labeled EW. The pressures listed in Table 3 are all relatively close in value (except for possibly SPT_3). SPT_6 is quite close to the predictions of CS and L, with all three being in good agreement with the simulation data (MC and EW). SPT_7 again yields pressures slightly above the other equations for $\eta > 0.25$, except for SPT_3, although SPT_7 is not much greater than the S and YK predictions. Presumably, a more accurate approximation for $g^{[3]}$, and hence the derivatives of $\bar{g}(1, 1)$, would lead to an improved SPT_7 prediction of P that might fall between the current SPT_6 and SPT_7 values.

Both Tables 2 and 3 demonstrate the successful incorporation of two new conditions into SPT. In particular, SPT_6 compares quite favorably with other equations of state, most of which are either empirical or semiempirical. One could argue that for $\eta \leq 0.50$ SPT_6 represents an improvement over most other equations of state except, perhaps, the CS and L equations. This conclusion is made more impressive given that, unlike most other hard sphere equations of state, the SPT method is a

TABLE 2: The Hard Sphere Fluid Pressure, $P\sigma^3/kT$, as a Function of Packing Fraction

η	MD	MD[29]	SPT_6	SPT_7	CS[14]	S[15]	YK[28]	SPT_3[1]
0.288	2.057[a] (1)	2.057	2.050	2.062	2.052	2.058	2.060	2.089
0.314	2.576[a] (1)	2.577	2.566	2.586	2.570	2.579	2.582	2.628
0.340	3.217[a] (1)	3.217	3.201	3.234	3.208	3.221	3.225	3.297
0.367	4.008[a] (1)	4.009	3.987	4.038	3.997	4.017	4.023	4.133
0.393	4.991[b] (1)	4.991	4.963	5.042	4.977	5.007	5.015	5.180
0.419	6.215[a] (1)	6.216	6.184	6.300	6.200	6.249	6.258	6.499
0.445	7.750[b] (2)	7.751	7.724	7.886	7.734	7.817	7.828	8.172
0.471	9.687[b] (3)	9.687	9.687	9.896	9.672	9.816	9.829	10.309
0.487	11.093[b] (4)	11.091	11.127	11.354	11.078	11.283	11.297	11.873
0.492	11.610[b] (4)	11.608	11.660	11.889	11.594	11.826	11.839	12.450

[a] The simulation calculations, MC, are 4 million cycles. The estimated uncertainties in the last significant figures are included in the parentheses [b] The simulation calculations, MC, for 20 million cycles. The estimated uncertainties in the last significant figures are included in the parentheses.

TABLE 3: The Hard Sphere Fluid Pressure, $P\sigma^3/kT$, as a Function of Packing Fraction

η	MC	EW[32]	SPT_6	SPT_7	L[30]	CS[14]	S[15]	YK[28]	SPT_3[1]
0.25	1.470[a] (1)	1.471	1.467	1.472	1.470	1.468	1.471	1.472	1.485
0.30	2.282[a] (1)	2.283	2.274	2.289	2.279	2.277	2.284	2.286	2.322
0.35	3.489[a] (1)	3.490	3.471	3.510	3.481	3.480	3.495	3.500	3.584
0.40	5.305[b] (1)	5.305	5.276	5.364	5.286	5.291	5.326	5.334	5.517
0.45	8.083[b] (2)	8.078	8.059	8.230	8.051	8.066	8.157	8.169	8.536
0.50		12.404	12.512	12.738	12.412	12.414	12.692	12.705	13.369

[a] The simulation calculations, MC, are 4 million cycles. The estimated uncertainties in the last significant figures are included in the parentheses [b] The simulation calculations, MC, for 20 million cycles. The estimated uncertainties in the last significant figures are included in the parentheses.

completely self-consistent theoretical approach, in which no adjustable parameters or simulation data are needed as input. (The equation of state obtained by Labik et al.[30] is also a self-consistent result. Their approach is different from ours, although interestingly, there appears to be a connection between the two methods.)

Finally, several hard sphere equations of state have been designed to replicate some or all of the (up to ten) known virial coefficients. It is therefore a common procedure to compare the predicted virial coefficients with the known coefficients. We do so in the Supporting Information. Although the virial expansion is convenient to use, it is ultimately the accuracy of the pressure predictions that matters, rather than the accuracy of the virial coefficient predictions (particularly at high density where even the virial expansion truncated after several terms begins to deviate from simulation data). In addition, other important fluid properties such as $g'(1^+)$, $g''(1^+)$, and $W(\lambda)$ are not easily found from equations of state based on the virial coefficients, whereas with SPT, they are easily determined, as is shown in the following subsections.

7.2 SPT Predictions of $g'(1^+)$ and $g''(1^+)$. The inclusion of more exact conditions on G leads to noticeable improvements over previous SPT results. In so doing, however, a relation between $G'(1)$ and $g'(1^+)$, for example, was needed. Although an exact connection between $G'(1)$ and $g'(1^+)$ was derived in section 4, an additional term, $\bar{g}(1, 1)$, appeared (eq 27). An approximation to $\bar{g}(1, 1)$ was obtained in section 5, where an initial set of simulations validated the use of the ideal gas approximation (eq 37) to estimate $\bar{g}(1, 1)$.

Here, we discuss another (indirect) test of our approximation for $\bar{g}(1, 1)$, as well as another check on the validity of the SPT method. We now compare the SPT_6 and SPT_7 predictions of the slope and curvature of the radial distribution function at contact with the results of molecular simulation. The self-consistently obtained expression for G from SPT_6 is substituted back into eq 37 to get $g'(1^+)$, whereas G from SPT_7, is substituted back into eqs 37 and 40 to find $g'(1^+)$ and $g''(1^+)$. We note, for example, that eq 37 contains a term that is proportional to $G(1)^2$. As the packing fraction increases, this term should therefore become more important. Because of this, we expect the resultant $g'(1^+)$ values to be more sensitive to the accuracy of G.

TABLE 4: The Slope of the Radial Distribution Function at Contact, $g'(1^+)$, at Various Fluid Fractions

η	MC	MC_2[31]	SPT_6	SPT_7	SPT_5[11]	L[30,31]
0.157	−1.59[a] (3)	−1.55(2)	−1.58	−1.60	−1.48	−1.58
0.209	−2.85[a] (2)	−2.80(3)	−2.85	−2.89	−2.52	−2.85
0.262	−4.91[a] (2)	−4.89(7)	−4.90	−5.00	−4.06	−4.88
0.314	−8.29[a] (4)	−8.17(10)	−8.26	−8.53	−6.37	−8.20
0.340	−10.77[a] (3)		−10.71	−11.13	−7.93	
0.367	−13.98[a] (2)	−13.86(13)	−14.02	−14.70	−9.86	−13.67
0.393	−18.21[b] (2)		−18.12	−19.11	−12.24	
0.419	−23.81[a] (3)	−23.64(27)	−23.74	−25.19	−15.21	−22.93
0.445	−31.27[b] (4)		−31.32	−33.40	−18.91	
0.471	−41.35[b] (4)	−41.26(1.34)	−41.75	−44.56	−23.57	−39.04

[a] The simulation calculations, MC, are 4 million cycles. The estimated uncertainties in the last significant figures are included in the parentheses [b] The simulation calculations, MC, for 20 million cycles. The estimated uncertainties in the last significant figures are included in the parentheses.

Table 4 lists the values of $g'(1^+)$ obtained from SPT_6 and SPT_7, from an integral equation derived by Labik et al.[30] and Smith et al.,[31] labeled L, and from simulations performed for this work (MC) and from ref 31 (MC_2). Additionally, Table 4 includes predictions from SPT_5, where $g'(1^+)$ is found directly from eq 16 using the value of $G'''(1/2)$ after $G(\lambda)$ has been solved for (using only five conditions). Our simulation calculations are in excellent agreement with the previous simulation values of ref 31 over the chosen range of fluid densities.

Overall, SPT_6 most accurately reproduces the simulation values for $g'(1^+)$. The L equation also does quite well at lower packing fractions but begins to underestimate the magnitude of the slope at higher packing fractions. In contrast, SPT_7 overestimates the magnitude of the slope as the packing fraction increases. Not surprisingly, both SPT_6 and SPT_7 show a marked improvement over SPT_5,[11] where the slope is consistently underestimated as the packing fraction increases. In SPT_6 and SPT_7, and unlike SPT_5, the approximate expression for $g'(1^+)$ is used self-consistently as another condition when solving for G.

TABLE 5: The Curvature of the Radial Distribution Function at Contact, $g''(1^+)$, at Various Packing Fractions

η	MC	MC_3[33]	SPT_6	SPT_7
0.157	3.0[a] (5)		11.2	3.0
0.209	7.3[a] (5)	1.7	22.3	7.2
0.262	16.2[a] (4)		42.5	16.7
0.314	35.8[a] (9)	29.1	79.5	37.7
0.367	78.7[a] (6)	64.8	153	86.5
0.393	117[b] (1)	90	204	129
0.419	176[a] (1)	143	283	195
0.445	264[b] (1)	197	394	299
0.471	400[b] (1)	293	557	461

[a] The simulation calculations, MC, are 4 million cycles. The estimated uncertainties in the last significant figures are included in the parentheses [b] The simulation calculations, MC, for 20 million cycles. The estimated uncertainties in the last significant figures are included in the parentheses.

The comparison between SPT_6 and L is interesting because both are derived from purely theoretical arguments. In fact, Labik et al.[30] applied a closure condition in their integral equation that involves both the three- and four-particle correlation functions, $g^{[3]}$ and $g^{[4]}$ (more specifically $y^{[3]}$ and $y^{[4]}$[30,31]). Despite our relatively simple closure, which includes only $g^{[3]}$, SPT_6 provides a better prediction of the slope of the radial distribution function at contact.

The curvature of the radial distribution function at contact, $g''(1^+)$, for various packing fractions is shown in Table 5. Included in this table are the predictions of SPT_6 and SPT_7 and simulation results obtained for this work (MC) and from Groot et al.[33] (MC_3). $g''(1^+)$ was determined from eq 40 for SPT_7. Because SPT_6 does not include eq 20 as another condition on G, $g''(1^+)$ was determined for SPT_6 by first generating the fourth derivative of G at $\lambda = {}^1/_2$ using the G obtained from six conditions only and then manipulating eq 20 to solve for $g''(1^+)$. The SPT_5 predictions of $g''(1^+)$ were quite inaccurate and are not included.

There is a definite discrepancy between our simulation results and the values given by Groot et al.[33] We also obtained different simulation estimates of $g'(1^+)$ than Groot et al., whose results underestimate the steepness of the slope at contact. Because our simulation results for $g'(1^+)$ are consistent with the data of ref 31 (MC_2 in Table 4) and the SPT_6 and L predictions, we are confident in our simulation estimates of $g''(1^+)$.

The SPT_7 predictions of $g''(1^+)$ are surprisingly good given the nature of the approximation used in its evaluation. SPT_7 is quite accurate at low packing fractions. The curvature is overestimated at higher packing fractions, although the results are not unreasonable. Because the curvature is not included as another condition, it is again not too surprising to see that SPT_6 does a poor job of reproducing $g''(1^+)$.

Overall, we can conclude that our approximation to $\bar{g}(1, 1)$ is robust enough to capture accurately the behavior of $g'(1^+)$ (at least as employed by SPT_6). However, the ideal gas approximation fails to capture the structure of $g^{[3]}$, which, although not required for predicting the average value $\bar{g}(1, 1)$, is a key missing ingredient for the accurate predictions of the various derivatives of $\bar{g}(1, 1)$. This missing information also serves to explain why the pressure and $g'(1^+)$ predictions of SPT_7 are not as accurate as those of SPT_6. Nevertheless, the fact that SPT_7 can predict the curvature of the radial distribution function at contact to within 15% of simulation results without any adjustable parameters is noteworthy.

The above results highlight the utility of SPT. Other semiempirical and empirical equations of state do not necessarily provide a clear route to obtaining properties of $g(r)$ other than its contact value. A recent paper by Robles and López de Haro[34] discusses the use of a so-called rational function approximation (RFA) method[35,36] in which the various derivatives of $g(1^+)$ can be generated from the compressibility factor, Z. The success of the method, however, depends on the choice of Z and which derivative is being evaluated. From the analyses presented in ref 34, $g'(1^+)$ and $g''(1^+)$ obtained from the CS equation of state were found to be more accurate than those obtained using the S equation of state. These results, however, still do not appear to be as accurate as the SPT_6 and SPT_7 predictions. Other choices for Z (for example, an equation proposed by by Ballance and Speedy[38]) also do not appear to match the accuracy of SPT_6 and SPT_7 for $g'(1^+)$, though some are of comparable accuracy for $g''(1^+)$.

TABLE 6: The Excess Chemical Potential, μ^{ex}/KT, of the Hard Sphere Fluid Obtained from Simulation and from Various Equations of State[a]

η	MC_5[40]	MC_6[41]	SPT_6	SPT_7	CS[14]	S[15]	YK[28]	SPT_3[1]
0.314	5.35(4)	5.35(3)	5.32	5.37	5.33	5.34	5.35	5.45
0.367	7.38(11)	7.36(4)	7.34	7.45	7.36	7.40	7.41	7.60
0.393	8.72(18)	8.61(3)	8.62	8.77	8.64	8.69	8.70	8.97
0.419	10.28(16)	10.20(3)	10.13	10.34	10.15	10.23	10.24	10.61
0.445	12.12(37)	12.08(5)	11.93	12.23	11.95	12.07	12.08	12.57
0.471	14.25(48)	14.1(2)	14.12	14.50	14.11	14.29	14.31	14.96
0.482	15.16(80)	14.9(2)	15.12	15.54	15.09	15.32	15.34	16.05
0.484	15.91(87)		15.39	15.81	15.35	15.58	15.61	16.34
0.487	15.69(1.03)		15.66	16.09	15.61	15.86	15.88	16.63
0.490	16.16(1.08)		15.93	16.37	15.88	16.14	16.16	16.93

[a] Estimated uncertainties in the last significant figures are included in the parentheses.

7.3 Work of Cavity Formation. The excess chemical potential, μ^{ex}, of the hard sphere fluid is equivalent to the reversible work of forming a cavity of radius $\lambda = 1$. The determination of μ^{ex} via eq 9 is straightforward once G is known. Likewise, the Gibbs−Duhem relation, eq 10, provides a simple route to the calculation of μ^{ex} from a given equation of state. Table 6 lists the various values of μ^{ex}/kT obtained from SPT and from other equations of state for moderate to high packing fractions. Also included in the table are the results of two different simulation methods. The values listed under the heading MC_5 were obtained with a MC simulation technique that uses the small system grand ensemble (SSGE).[40] The values in the column MC_6 are MC simulation results calculated using the force-balance method.[41]

Because SPT_6 slightly underestimates the pressure, it also yields values of μ^{ex}/kT that are slightly below the SSGE simulation results. The opposite occurs for SPT_7, which slightly overestimates the excess chemical potential. Nevertheless, both sets of predictions are statistically indistinguishable from the SSGE simulation results and are markedly improved over the SPT_3 results. Interestingly, SPT_6 and CS yield nearly identical values of μ^{ex}/kT.

The SPT_6 values are slightly lower than the other equation of state predictions, except for $\eta > 0.46$, where SPT_6 slightly exceeds CS. SPT_7 predictions are consistently higher than the other results, except for SPT_3. Both sets of simulation data seem to be in better agreement with the S and YK predictions, although the uncertainties of the simulation values at packing fractions near the freezing transition ($\eta > 0.471$) make it difficult to distinguish between all the equations of state.

The reversible work of forming a cavity with a radius other than $\lambda = 1$ is another quantity that is easily generated once G has been solved for. In contrast, the various empirical and semiempirical equations for the compressibility factor Z do not conveniently provide, if at all, property predictions beyond those

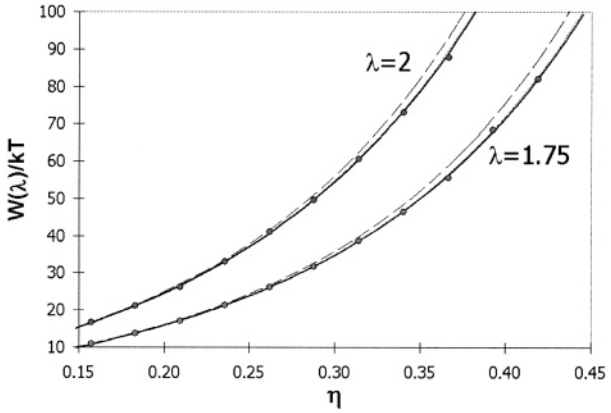

Figure 6. Reversible work of cavity formation, $W(\lambda)/kT$, versus packing fraction, η, for cavity radii of $\lambda = 1.75$ and 2. The symbols are the simulation values obtained for this work. The dashed upper line is the equation from ref 42. The middle line is the equation from ref 43. The bold lower line represents the prediction of SPT_6. On the scale of this plot, ref 43 and SPT_6 are nearly indistinguishable.

which they were designed to produce (such as P and μ^{ex}). Hence, to assess the accuracy of our SPT results, we need to compare our predictions with the results of methods other than those we have already discussed. For example, Chen and Weeks[42] present a number of different, but related, routes toward the determination of the free-energy differences needed to insert hard sphere solutes of different sizes within a hard sphere solvent. Their method makes use of a set of field equations and invokes either a Hydrostatic Linear Response (HLR) model or the Gaussian Field Model (GFM). They found that the best results for the work of insertion came from using HLR with the compressibility route.[42] Because the compressibility route also provides an analytical expression, we include its prediction for comparison. We note, however, that this equation is identical to the SPT_3 expression for $W(\lambda)/kT$. Another method for generating the work of cavity formation is a semiempirical approach developed by Matyushov and Ladanyi (ML).[43] The ML method uses a third-order polynomial in the cavity radius to describe the reversible work of cavity formation. The coefficients of the polynomial expansions are chosen such that the $\lambda = 1$ result matches the excess chemical potential of the CS equation of state and that the correct asymptotic behavior at the infinite dilution limit (known from SPT) is attained.

We compare the predictions of $W(\lambda)/kT$ for $\lambda = 1.75$ and 2 from SPT_6, the HLR equation,[42] and ML[43] with simulation results in Figure 6. We do not include SPT_7 predictions because both the pressure and chemical potential obtained from SPT_7 are not as accurate as those obtained from SPT_6. The SPT_6 and ML predictions are nearly identical (at least on the scale of the plot), and both match the simulation results quite well. The HLR predictions of $W(\lambda)/kT$ are, however, too high at moderate to high packing fractions. For $\lambda \leq 1.25$ and up to packing fractions of $\eta = 0.445$, all three approaches were in excellent agreement with simulation. For cavity radii within the range of $1.25 < \lambda < 1.75$, similar trends, as seen in Figure 6, were observed. Because the correct infinite dilution limits are automatically included within SPT, the SPT_6 values for $W(\lambda)/kT$ match both the ML and simulation results extremely well.

A systematic test of all methods for larger cavity radii is not feasible due to the large simulations needed to generate $W(\lambda)/kT$ for $\lambda > 2$ at moderate to high densities. Simulation results are known, however, for some particular values of λ and η. For example, for a cavity of radius $\lambda = 3$ and $\eta = 0.2$, the simulation gives $W(\lambda)/kT = 89.2$,[46] SPT_6 predicts $W(\lambda)/kT = 89.4$, ML yields $W(\lambda)/kT = 89.4$, and CW gives a result of $W(\lambda)/kT = 90.3$. Within the inherent uncertainty of the simulation results, SPT_6 and ML both accurately reproduce the simulation values.

8. Conclusions

The addition of two new constraints on the form of G results in marked improvements to the accuracy of SPT. The pressure, excess chemical potential, and reversible work of cavity formation generated by SPT_6, in particular, are in excellent agreement with the results of molecular simulation. This agreement is made all the more impressive given that we have started from first principles and have maintained throughout a self-consistent framework. Overall, the introduction of new conditions now makes SPT competitive with other approaches.

Because our extension of SPT is reliant upon a fair number of physically and geometrically based arguments, there is a high likelihood that further improvements to the current versions of SPT_6 and SPT_7 can be made. Advances must, of course, begin with better predictions of $\bar{g}(1, 1)$, particularly its derivatives. Information on the detailed structure of $g^{[3]}$ is therefore required, although only for the case in which three spheres are in or near rolling contact. We note here that our chosen closure for $g^{[3]}$ is very similar to the first-order approximation utilized in refs 30 and 31. These authors also propose a higher-order approximation that yields better agreement with simulation. One could also revisit the application of eq 32 but instead consider both the volume and surface area contributions to the work of cavity formation. Some initial calculations performed by us suggest that the oscillatory nature of $g^{[3]}$ is reproduced when the surface tension term is included. Because $\bar{g}(1, 1)$ is already well described by the ideal gas approximation, better approximations to $g^{[3]}$, however, would most likely yield improvements to SPT_7, with only minor improvements to SPT_6.

Other conditions on G, beyond the seven already applied, could be obtained in a straightforward manner by the continued differentiation of eq 14. Although formally exact, each additional derivative introduces another unknown quantity. Separate and approximate closures are required to evaluate these unknown quantities before the new conditions can be incorporated into SPT. Consequently, these new relations (like the sixth and seventh conditions derived in the paper) would not form a completely closed set of SPT conditions. For example, the expression for the fifth derivative of G, $G^{(5)}(1/2 + \epsilon)$ (a potential eighth condition), would contain the third derivative of $g(1^+)$, $g'''(1^+)$ (as well as $g''(1^+)$ and $g'(1^+)$), which would need to be approximated before the condition could be applied. The generation of new conditions in this manner may be of limited utility.

Finally, the success of SPT_6 and SPT_7 for the pure component hard sphere fluid suggests that a similar extension of SPT for multicomponent hard sphere mixtures can be made. To date, only three corresponding exact conditions have been applied for the additive binary hard sphere mixture,[44] which constrain the forms of the two functions G_A and G_B (where A and B represent the two types of particles). Because the SPT integral equation can be extended to the binary mixture, the possibility exists for deriving all seven analogous conditions on G_A and G_B.

Acknowledgment. We are grateful for the financial support of the Shreve Trust, Purdue Research Foundation.

Supporting Information Available: Derivation of five SPT exact conditions (three of which have been previously found,

two of which are new) is presented in Section 2 as well as the derivatives of $\bar{g}(1, 1)$ that were used in Section 5. Also, a table of virial coefficients predicted by SPT and other equations of state is included. This material is available free of charge via the Internet at http://pubs.acs.org.

References and Notes

(1) Reiss, H.; Frisch, H. L.; Lebowitz, J. L. *J. Chem. Phys*. **1959**, *31*, 369.
(2) Stillinger, F. H. *J. Solution Chem*. **1973**, *2*, 141.
(3) Irisa, M.; Nagayama, K.; Hirata, F. *Chem. Phys. Lett.* **1993**, *207*, 430.
(4) Floris, F. M.; Selmi, M.; Tani, A.; Tomasi, J. *J. Chem. Phys*. **1997**, *107*, 6353.
(5) Punnathanam, S.; Corti, D. S. *Ind. Eng. Chem. Res.* **2002**, *41*, 1113.
(6) Reiss, H. *Statistical Mechanics and Statistical Methods in Theory and Application*; Plenum: New York, 1976.
(7) Reiss, H.; Casberg, R. V. *J. Chem. Phys.* **1974**, *61*, 1107.
(8) Speedy, R. J. *J. Chem. Soc., Faraday Trans. 2*. **1977**, *73*, 714.
(9) Speedy, R. J. *J. Chem. Soc., Faraday Trans.* **1981**, *77*, 329.
(10) Reiss, H. *J. Phys. Chem*. **1992**, *96*, 4736.
(11) Mandell, M. J.; Reiss, H. *J. Stat. Phys*. **1975**, *13*, 113.
(12) Stillinger, F. H.; Cotter, M. A. *J. Chem. Phys*. **1971**, *55*, 3349.
(13) Speedy, R. J. *J. Chem. Soc., Faraday Trans*. **1980**, *76*, 693.
(14) Carnahan, N. F.; Starling, K. E. *J. Chem. Phys*. **1969**, *51*, 635.
(15) Sanchez, I. *J. Chem. Phys.* **1994**, *101*, 7003.
(16) Reiss, H.; Ellerby, H. M.; Manzanares, J. A. *J. Phys. Chem*. **1996**, *100*, 5970.
(17) Chua, L. P. M.S. Thesis, Purdue University, West Lafayette, IN, 2001.
(18) Widom, B. *J. Stat. Phys*. **1978**, *19*, 563.
(19) Attard, P.; Stell, G. *Chem. Phys. Lett*. **1992**, *189*, 128.
(20) Bellemans, A.; Orban, J. *Chem. Phys. Lett*. **1968**, *2*, 253.
(21) Corti, D. S.; Reiss, H. *Mol. Phys.* **1998**, *95*, 269.
(22) Asakura, S.; Oosawa, F. *J. Chem. Phys.* **1954**, *22*, 1255. Asakura, S.; Oosawa, F. *J. Polymer Sci.* **1958**, *33*, 183.
(23) Roberts, A. P.; Knackstedt, M. A. *Phys. Rev. E* **1996**, *54*, 2313.
(24) Smit, B.; Frenkel, D. *Understanding Molecular Simulation*; Academic: San Diego, CA, 1996.
(25) Press, W. H.; Teukolsky, S. A.; Vetterling, W. T.; Flannery, B. P. *Numerical Recipes*, 2nd ed.; Cambridge University Press: New York, 1992.
(26) Mulero, A.; Faúndez, C. A.; Cuadros, F. *Mol. Phys*. **1999**, *96*, 453.
(27) Miandehy, M.; Modarress, H. *J. Chem. Phys*. **2003**, *119*, 2716.
(28) Yelash, L. V.; Kraska, T. *Phys. Chem. Chem. Phys*. **2001**, *3*, 3114.
(29) Kolafa, J.; Labık, S.; Malijevsk×c6, A. *Phys. Chem. Chem. Phys*. **2004**, *6*, 2335.
(30) Labık, S.; Malijevsk×c6, A.; Smith, W. R. *Mol. Phys*. **1994**, *83*, 983.
(31) Smith, W. R.; Labık, S.; Malijevsk×c6, A.; Šedlbauer, J. *Mol. Phys*. **1994**, *83*, 1223.
(32) Erphenbeck, J. J.; Wood, W. W. *J. Stat. Phys*. **1984**, *35*, 321.
(33) Groot, R. D.; van der Eerden, J. P.; Faber, N. M. *J. Chem. Phys*. **1987**, *87*, 2263.
(34) Robles, M.; López de Haro, M. *J. Chem. Phys*. **1997**, *107*, 4648.
(35) Bravo Yuste, S.; Santos, A. *Phys. Rev. A* **1991**, *43*, 5418.
(36) Bravo Yuste, S.; López de Haro, M.; Santos, A. *Phys. Rev. E* **1996**, *53*, 4820.
(37) Henderson, D.; Grundke, E. W. *J. Chem. Phys.* **1975**, *63*, 601.
(38) Ballance, J. A.; Speedy, R. J. *Mol. Phys*. **1985**, *54*, 1035
(39) Janse van Rensburg, E. J. *J. Phys. A* **1993**, *26*, 4805.
(40) Heying, M.; Corti, D. S. *Fl. Phase. Equil.* **2003**, *204*, 183.
(41) Attard, P. *J. Chem. Phys*. **1993**, *98*, 2225.
(42) Chen, Y.; Weeks, J. D. *J. Chem. Phys*. **2003**, *118*, 7944.
(43) Matyushov, D. V.; Ladanyi, B. M. *J. Chem. Phys.* **1997**, *107*, 5815.
(44) Lebowitz, J. L.; Helfand, E.; Praestgaard, E. *J. Chem. Phys*. **1965**, *43*, 774.
(45) McQuarrie, D. A. *Statistical Mechanics*; University Science Books: Sausalito, CA, 2000.
(46) Siderius, D. Personal communication.